

A Holistic Optimization Framework for Energy Efficient UAV-assisted Fog Computing: Attitude Control, Trajectory Planning and Task Assignment

Shuaijun Liu, Jinqiu Du, Yaxin Zheng, Jiaying Yin, Yuhui Deng, Jingjin Wu, *Member, IEEE*

Abstract—Unmanned Aerial Vehicles (UAVs) have significantly enhanced fog computing by acting as both flexible computation platforms and communication mobile relays. In this paper, we propose a holistic framework that jointly optimizes the total latency and energy consumption for UAV-assisted fog computing in a three-dimensional spatial domain with varying terrain elevations and dynamic task generations. Our proposed framework considers three important and interdependent modules: attitude control, trajectory planning, and task assignment. We first establish a fuzzy proportional-integral-derivative control model to determine the UAV's attitude. Then, we propose an enhanced Ant Colony System (ACS) based algorithm, that includes a safety value and a decoupling mechanism to overcome the convergence issue in classical ACS, to compute the optimal UAV trajectory. Finally, we design an algorithm based on the Particle Swarm Optimization technique, to determine where each offloaded task should be executed. Under our proposed framework, the outcome of one module would affect the decision-making in one other, providing a holistic perspective of the system and thus leading to improved solutions. We demonstrate by extensive simulation results that our proposed framework can significantly improve the overall performance, measured by latency and energy consumption, compared to existing baseline approaches.

Index Terms—Fog Computing, Unmanned Aerial Vehicles (UAV), Attitude Control, Trajectory Planning, Ant Colony Algorithm

I. INTRODUCTION

Driven by the development of the Internet of Things (IoT) [1], mobile terminal devices such as smartphones and tablets are now capable of generating and collecting massive amounts of data. However, the ability of processing these data, such as performing computational tasks, in the IoT devices are still limited [2], [3]. On the other hand, Unmanned Aerial Vehicles (UAVs) have been recently identified as a versatile platform that connects IoT devices and servers or data centers

via the network edge [4]. In addition, some UAVs are equipped with computational capabilities and thus can be regarded as “moving fog nodes” for offloading certain computational tasks. To fully utilize the versatility and flexibility of UAVs in fog computing, key considerations include the management of each UAV's attitude, the strategic planning of their respective trajectories, and the efficient task assignment policy to determine the appropriate computing device for each task.

This paper considers a fog computing environment with a single UAVs deployed at the network edge, aiming at maximizing the energy efficiency by collaboratively controlling the attitudes and planning the trajectories, as well as determining the location for each computing task to be executed. Without loss of generality, we focus on quadrotor UAVs, which are considered ideal for computation offloading in IoT networks due to their enhanced flexibility [5]–[8].

Attitude control, trajectory planning, and task assignment policy in UAV-assisted fog computing are very important processes that significantly impact the overall efficiency of the system [9]–[11]. Specifically, **attitude control** (by adjusting pitch, roll, and yaw) ensures a stable and precise orientation of the UAV during operation, which is a necessary condition to maintain a high quality of communication with IoT devices and other fog nodes [12]. In addition, a stable attitude facilitates the UAV to effectively perform computation and storage tasks as a fog node. On the other hand, **trajectory planning** of the UAV can reduce its power consumption by identifying the most efficient path to collect data and tasks based on the locations of IoT devices [13]. Finally, **task assignment** refers to the process of deciding whether a specific task should be handled locally by the IoT device, processed in the fog layer (including the UAV), or offloaded to the central cloud. Specific objectives, including minimizing latency, maximizing throughput, or optimizing energy efficiency, can be achieved by smartly assigning tasks to appropriate devices. Task assignment is often jointly optimized with **resource allocation**, where transmission resources such as power and bandwidth are distributed among different transmission pairs in the network, to facilitate the transmission process and improve the overall efficiency. The four processes are inherently linked in UAV-assisted fog computing. For example, a UAV's attitude control would ensure that it maintains optimal orientations while following a planned trajectory or processing a task. Also, when deciding whether to offload a certain task to the fog or the cloud and how to allocate

A preliminary version of this paper was presented at IEEE HPCC 2022 in December 2022, and was included in its proceedings (DOI: 10.1109/hpcc-dss-smartcity-dependsys57074.2022.00217).

S. Liu, is with the Department of Applied Data Analysis, Boston University, Boston MA, USA. (Email: shuaijun@bu.edu).

J. Du and Y. Zheng are with the Department of Statistics and Data Science, BNU-HKBU United International College, Zhuhai, Guangdong, China (Email: turbodddu@gmail.com, kristenzyx@163.com).

J. Yin is with the School of Clinical Medicine, University of Cambridge, CB2 0SP Cambridge, U.K. (E-mail: jy517@cam.ac.uk).

Y. Deng and J. Wu are with the Department of Statistics and Data Science, BNU-HKBU United International College, Guangdong, China, and also with the Guangdong Provincial Key Laboratory of Interdisciplinary Research and Application for Data Science, Guangdong, China (Email: ivandeng@uic.edu.cn, jj.wu@ieee.org). Corresponding author: J. Wu.

relevant transmission resources, the energy consumption and latency for a certain UAV to reach the proximity of the IoT initiating the task along a planned trajectory should also be taken into account.

Existing studies have considered two or three processes for joint optimization. For example, Wei *et al.* [14] proposed three decision-making algorithms to solve the joint optimization problem involving energy consumption and mean delay. Our previous published conference paper [15] considered the joint optimization of trajectory planning and task assignment, in a fog computing system assisted by one single UAV. We proposed an optimization framework that integrated the classical Ant Colony System (ACS, also referred as Ant Colony Optimization/ACO in some existing studies) and Particle Swarm Optimization (PSO) algorithms. The framework would generate the optimal trajectory in a two-dimensional plane with randomly generated computing tasks and obstacles, and decide the optimal location (the IoT device, the UAV, or the central cloud) for each task to be executed.

In this work, we revise and extend the model in [15] to better align with the practical scenarios of UAV-assisted fog computing. Particularly, we consider a three-dimensional network space (compared to a two-dimensional plane as in [15]) with varying terrain elevations. We also add the attitude control and optimal structure design modules for a quadrotor UAV, to ensure the stability of flights, prevent potential structural damage, and reduce the latency when the UAV ascends or descends by two newly proposed Active Disturbance Rejection Control (ADRC) strategies [16]. Compared to most existing similar studies, (e.g., [6]–[8], [17], [18]), which only considered the trajectory planning and flight attitude at independent static points, we jointly consider planning the optimal trajectory and determining the attitudes, taking into account the extra consumption required for changing attitude along the trajectory. Our research is expected to provide new useful insights in UAV-assisted fog computing applications for improving the overall performance and efficiency.

The contributions of this paper are summarized as follows.

- We propose a holistic framework with multiple modules including attitude control, trajectory planning, resource allocation, and task assignment, to optimize the overall energy efficiency for UAV-assisted fog computing in a three-dimensional spatial domain with varying terrain elevations. To the best of our knowledge, this is the first work that jointly considers these modules together and takes advantage of their intricate interconnections. By integrating and coordinating the modules, our proposed framework is capable of achieving optimal performance and energy efficiency in the dynamic and complex environment of UAV-assisted fog computing.
- We establish a fuzzy proportional-integral-derivative control (PID) model for quadrotor UAV attitude control. Compared to the classical PID control commonly used in existing studies, the fuzzy PID control can capture the dependencies among parameters and adapt to the dynamic environment. We demonstrate that the fuzzy PID control

can effectively improve the stability in takeoff, cruise, and landing phases, and thus reduce both latency and energy consumption in UAV-assisted fog computing.

- We propose a computationally efficient algorithm called ACS-DS (ACS with Decoupling and Safety values), to incorporate two mechanisms for decoupling and safety values in the ACS algorithm, to overcome the common issues of slow convergence and trapped in local optimum in classical ACS in UAV trajectory planning problems. We prove the convergence of the proposed algorithm and show that it has a polynomial time complexity. We also verify its superiority in terms of the convergence performance over classical ACS by numerical experiments.
- We propose a heuristic algorithm based on the idea of PSO to solve the joint optimization problem involving resource allocation and task assignment in UAV-assisted fog computing, given that an initial trajectory of the UAV has been determined. The heuristic algorithm is shown to be capable of overcoming the complexities in the non-convex optimization problem and obtaining the optimal task assignment and resource allocation decisions efficiently.
- We demonstrate, through extensive numerical experiments, that our proposed holistic framework can reduce overall operational efficiency cost by more than 58% compared to baseline implementations.

The rest of this paper is organized as follows. Section II reviews recent advancements on attitude control, trajectory planning, and task assignment in UAV-assisted fog computing. Section III provides descriptions on the UAV architecture as well as key metrics at the system level. Section IV explains the formulation of the joint optimization problem. Section V describes the proposed computationally efficient algorithms to solve the problem in detail. Section VI demonstrates the improvements of the proposed algorithm by extensive numerical results. Section VII concludes the paper.

II. RELATED WORK

The fuzzy proportional-integral-derivative (PID) control system was adopted in attitude control and trajectory planning processes [19], [20]. It has been demonstrated that a proper combination of proportional-integral (PI) and proportional-derivative (PD) values and an optimally tuned fuzzy gain can better stabilize and control the attitude of quadrotor UAVs, as well as track their trajectories with smaller errors.

For trajectory planning of UAVs, heuristic algorithms such as PSO [21], ACS [22], and genetic algorithm (GA) [23], have been adopted to overcome the space and computation complexities in such problems. Compared with another branch of approaches that use neural networks and deep learning as the key techniques (e.g., [24]–[26]), heuristic algorithms are more interpretable and less data dependent, and thus more appropriate for UAV-assisted fog computing scenarios where the operational environments are usually highly diverse and dynamic, and transparent heuristics are preferred for regulators to validate and verify the operation. Among the heuristic

algorithms, the PSO [27] is one of the most commonly used techniques in such problems. However, one major concern of applying PSO in complex systems is that PSO may be converged prematurely to local optima [28].

ACS, based on the study of ants searching for food, is another commonly adopted technique in discrete and continuous optimization problems [29], [30]. While ACS-based approaches are well-known for their robustness, they also suffer the disadvantage of being prone to local optima due to premature convergence like PSO. To overcome this issue, Ali *et al.* proposed the maximum-minimum ACS that improved the performance at the expense of slower convergence speed [31]. In addition, Wang *et al.* [32] presented an adaptive double-layer ant colony optimization algorithm (DL-ACS) based on an elitist strategy (ADAS) and an improved moving average algorithm (IMA) to solve a three-dimensional UAV trajectory planning problem. Liu *et al.* [33] also proposed an efficient online path-planning algorithm based on DL-ACS, that was shown to improve the optimal solution and convergence speed concurrently, and to enhance the stability of the algorithm.

Meanwhile, resource allocation or task assignment problems have been extensively studied in existing studies. For example, Cui *et al.* [34] proposed a multi-agent Q-learning-based reinforcement learning (MARL) framework, where each agent independently executes the allocation algorithm to optimize the overall energy efficiency. Li *et al.* [35] considered a joint optimization problem involving trajectory optimization and task allocation, with the goal of minimizing UAV energy consumption and optimizing computation offloading and using successive convex approximation (SCA) technique to solve it. Wu *et al.* [36] proposed a cooperative multi-agent deep reinforcement learning framework, which combines task assignment and allocation of limited communication resources to minimize the overall energy consumption and delay.

In trajectory planning and/or task assignment problems, one notable issue of applying ACS or PSO is that the algorithm may enter the deadlock state where one or more tasks wait endlessly for resources [37]. Zhou *et al.* [38] and Hou *et al.* [39] both proposed ACS-based algorithms with enhanced communication mechanisms to avoid deadlocks. While the proposed methods managed to reduce the likelihood of deadlocks, they did not eliminate the possibilities of such undesirable events. Another effort to overcome the deadlock problem is to establish a *dead-corner table* (or referred as a *dead angle table*) [40], which updates the path strength using a penalty function to avoid the deadlock. While this approach effectively overcomes the deadlock problem, it introduces additional overheads in maintaining the table and thus is less efficient.

Another popular emerging approach to solve UAV-related planning and optimization problem is the deep reinforcement learning (DRL) (e.g., [41], [42]). However, we focus on classical heuristic algorithms (such as ACS and PSO), as they are known to be more scalable, more adaptive and less computationally intensive compared to DRL-based approaches [43]. These advantages make them particularly well-suited for the dynamic and large-scale nature of UAV-assisted fog computing

scenarios.

Our work in this paper combines the techniques mentioned above that have been demonstrated to be effective in respective processes, including fuzzy PID attitude control, ACS-based trajectory planning, and PSO-based task allocation and resource allocation. Following this foundation, we further improve several aspects of the entire framework, such as 1) the hardware of the quadrotor is designed to match the efficient performance of the fuzzy PID control system, 2) two enhanced anti-lockout mechanisms (decoupling and safety values) in the classical ACS for trajectory planning, and 3) a modified PSO approach with improved efficiency that is more appropriate for task assignment and resource allocation in large-scale UAV-assisted fog computing systems.

III. SYSTEM MODEL

A. Network Structure and Components

We consider a UAV-assisted fog computing system in a three-dimensional Euclidean space. The system consists of a quadrotor UAV, a remote data center (DC) in the cloud, and K mobile IoT devices (MDs). A demonstration of the key structures in the system is shown in Fig. 1.

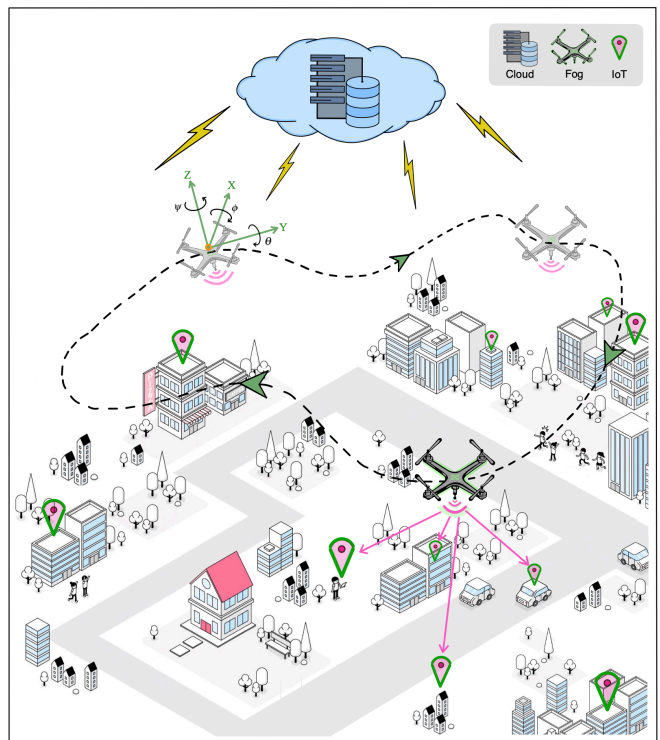


Fig. 1: The structure of UAV-assisted fog computing network.

The positions of K MDs are randomly distributed according to a Poisson Point Process (PPP), with the coordinate of the j th MD denoted by $M_j = [x_j, y_j, z_j]$. For convenience, we discretize a continuous time horizon with length T uniformly into N timeslots, and thus each timeslot has a length of $L = \frac{T}{N}$. We assume that N is sufficiently large, or equivalently, the timeslots are sufficiently short, such that the position of the

TABLE I: A summary and comparison of related studies

| Research | Process(es) focused | Method(s) | Objective(s) |
|------------------|---|----------------------------------|--|
| [34] | Trajectory Planning & Task Assignment | MARL | Max. long-term rewards |
| [35] | Trajectory Planning & Task Assignment | SCA | Max. UAV energy efficiency |
| [9] | Trajectory Planning & Task Assignment | Convex Optimization | Min. energy consumption and latency |
| [21] | Task Assignment | PSO | Min. the overall workflow execution cost |
| [23] | Task Assignment | GA | Min. communication costs |
| [14] | Task Assignment | Reinforcement learning | Max. the platform's utility |
| [31] | Trajectory Planning | MMACS | Min. route length while avoiding collision |
| [28] | Trajectory Planning | Multi-Swarm PSO | Max. the survivability of UAV |
| [33] | Trajectory Planning | Double-layer ACS | Max. the distribution efficiency |
| [32] | 3D-Trajectory Planning | Double-layer ACS | Max. Allocation Efficiency |
| [33] | Trajectory Planning | Double-layer ACS | Max. Allocation Efficiency |
| [38], [39] | Trajectory Planning | Enhanced ACS | Avoid path deadlock |
| [44], [40], [45] | Trajectory Planning | Enhanced ACS & Dead-corner table | Avoid path deadlock & Min. Task transfer latency |
| [19] | Attitude Control | Traditional PID controller | Control attitude |
| [20] | Trajectory Planning & Attitude Control | Fuzzy PID controller | Control attitude and track trajectory |
| [36] | Task Assignment | Reinforcement learning | Min. energy consumption and latency |
| Our Work | 3D Trajectory Planning & Task Assignment & Attitude Control | PSO & Fuzzy control & ACS-DS | Min. energy consumption and latency |

TABLE II: Key notations in the system model

| Notation | Definition |
|--------------------------|--|
| K | The total number of MDs |
| L | The length of every timeslot |
| T | The total number of timeslots required to complete all tasks |
| (x_j, y_j, z_j) | The location of the j th MD |
| $(x(t), y(t), z(t))$ | The location of the UAV at the t th timeslot |
| $\mathbf{v}(t)$ | The UAV's velocity vector at the t th timeslot |
| $d_j(t)$ | The distance between the UAV and j th MD at the t th timeslot |
| B_c | The battery capacity of the UAV |
| N_j | The total number of tasks from the j th MD |
| N_c | The total number of wireless channels |
| $C_j(t)$ | The number of channels assigned to the j th MD at the t th timeslot |
| N_b | The number of UAV propeller blades |
| R | The radius of UAV propeller blades |
| γ | The mounting angle of UAV propeller blades |
| P_w, P_t | Width and thickness of UAV propeller blades |
| $p_u(t), p_D(t), p_j(t)$ | The transmission power of the UAV, the DC, or the j th MD at the t th timeslot |
| $f(t), f_j(t)$ | The processing frequency of equipment for UAV, or the j th MD at the t th timeslot |
| $\mathbb{S}(t)$ | The weighted sum of network energy consumption and delay at the t th timeslot |

UAV can be considered to be fixed within each timeslot. We use $[x(t), y(t), z(t)]$, where $t \in \{1, 2, \dots, N\}$, to denote the position of the UAV at the t th timeslot. The UAV is powered by a battery with a maximum capacity of B_c . The height and speed are restricted to not exceed z^{\max} and v^{\max} , respectively, at all times.

We consider that task arrivals from each MD conform to a Poisson process, with an arrival rate λ_j from the j th MD. We use $s_{ij}(t)$, which is assumed to be exponentially distributed, to denote the data size of the i th task from the j th MD to be processed at the j th timeslot, and c_{ij} to denote the number of CPU cycles required to process the task.

As we introduced in [15], the proportion of channels allocated to the j th MD would be based on the Gamma distribution,

$$P_j(t) = \frac{\beta^\alpha}{(\alpha - 1)!} s_{ij}(t)^{\alpha-1} e^{-\beta s_{ij}(t)}, \quad (1)$$

where α and β are the shape and rate parameters in the Gamma distribution. For demonstration purposes, we set $\alpha = \beta = 2$ throughout the paper. Given the total number of available channels N_c , the number of channels allocated to the j th MD at the t th timeslot is $C_j(t) = \lceil N_c \cdot P_j(t) \rceil$ where $\lceil x \rceil$ rounds x to the nearest integer. The rationale of this arrangement is to prevent the channel from being monopolized by extremely large tasks, and thus to ensure a certain level of transmission efficiency for all tasks.

For the i th task from the j th MD, we denote the energy consumption and delay as E_{ij} and D_{ij} , respectively. For each task, the quadrotor UAV needs to move sufficiently close to the MD that initiates the task through a planned trajectory, in order to receive and further process the task. As mentioned earlier, a task may be executed locally, in the fog layer by the UAV, or further offloaded to the data centers in the central cloud. The computing results of any offloaded task need to be transmitted back to the initiating MD. In this context, we define $\mathbf{o}_{ij}(t) = (o_{ij}^{\text{MD}}(t), o_{ij}^{\text{UAV}}(t), o_{ij}^{\text{DC}}(t))$ as an array consisting of binary variables that indicate the specific execution location of the i th task from the j th MD during the t th timeslot. For ease of reference, we list the key notations related to the system model in Table II.

B. The Controllable Structure of Quadrotor UAV

Quadrotor UAVs are capable of achieving six degrees of freedom in pitch, yaw, roll, vertical, fore and aft, and lateral motion by translating and rotating along the x , y and z axes.

The process is accomplished by controlling four kinetic input quantities of the motor, denoted by $\mathbf{U} = (U_1, U_2, U_3, U_4)^T$, and six output control variables that include the changes of movements $\mathbf{v} = (\Delta x, \Delta y, \Delta z)$ on the x , y , and z directions, and the changes of attitude angles $\mathbf{A} = (\Delta \phi, \Delta \theta, \Delta \psi)$ resulting from rotation on the three axes.

Specifically, \mathbf{v} stands for linear velocity, which is the speed at which the UAV moves in real space and determines the location and speed of the UAV in the map. \mathbf{A} represents the angular velocity, rotates around three axes (x , y and z) and determines the attitude change and the turning speed of the UAV.

According to the Newton-Euler theorem, the nonlinear dynamics equations of a quadrotor UAV are [18],

$$\begin{cases} \ddot{x}(t) = \frac{1}{m}U_1(t)(\sin\phi\sin\psi + \cos\phi\sin\theta\cos\psi) \\ \ddot{y}(t) = \frac{1}{m}U_1(t)(-\sin\phi\sin\psi + \cos\phi\sin\theta\sin\psi) \\ \ddot{z}(t) = \frac{1}{m}U_1(t)(\cos\phi\cos\theta) - g \\ \ddot{\phi}(t) = \frac{1}{I_x}(lU_2(t) - \dot{\theta}\dot{\psi}(I_z - I_y)) \\ \ddot{\theta}(t) = \frac{1}{I_y}(lU_3(t) - \dot{\phi}\dot{\psi}(I_x - I_z)) \\ \ddot{\psi}(t) = \frac{1}{I_z}(U_4(t) - \dot{\phi}\dot{\theta}(I_y - I_x)) \end{cases} \quad (2)$$

where the left hand side of each equation represents the second order derivative of the relevant variable with respect to t . I_x , I_y , and I_z are the rotational inertia of the UAV body around its own x , y , and z axes, respectively. I_x and I_y are approximated based on the assumption of structural symmetry of the quadrotor UAV. Meanwhile, l is the distance from the center of mass of the body to the center of the rotor, which is also equal to half of the airframe wheelbase.

Fig. 2 shows the schematic diagram of a quadrotor UAV in motion. Two pairs of motors ($M1, M4$) and ($M2, M3$) rotating in opposite directions are used to eliminate counter-torque. Moreover, m is the mass of the UAV. g is the acceleration of gravity, I_x , I_y , and I_z are the rotational inertia of the UAV body around x , y , and z axes, respectively.

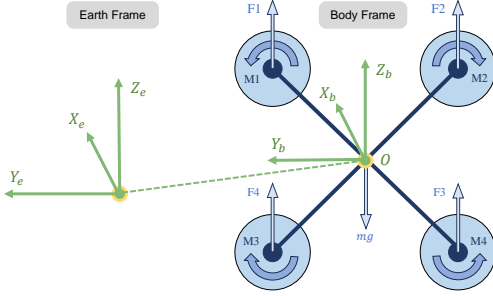


Fig. 2: Schematic diagram of a quadrotor UAV in motion

The input and output quantities interact with each other to change the UAV motion by adjusting the rotational speed of the four rotors (propellers). The trusts $F_i(t)$, ($i = 1, 2, 3, 4$) provided by the motors are directly proportional to the square of the angular velocity of the rotors (propellers) of the corresponding motors $\omega_i(t)$, ($i = 1, 2, 3, 4$), namely,

$$F_i(t) = C_T(t)\omega_i(t)^2, \quad (3)$$

where $C_T(t)$ is the trust coefficient of the propellers. The torque representing the magnitude of the torque to overcome the air resistance is given by

$$M_p(t) = C_M(t)\omega_i(t)^2, \quad (4)$$

with $C_M(t)$ as the torque coefficient.

For more details on principles related to attitude control and the calculation of the dynamics input \mathbf{U} , see Appendix A.

C. Rotor Propeller Design of Quadrotor UAV

We now introduce the factors that would affect $C_T(t)$ and $C_M(t)$. The propeller is the power source of the UAV. Fig. 3 shows the structure of the quadrotor UAV propeller, where the

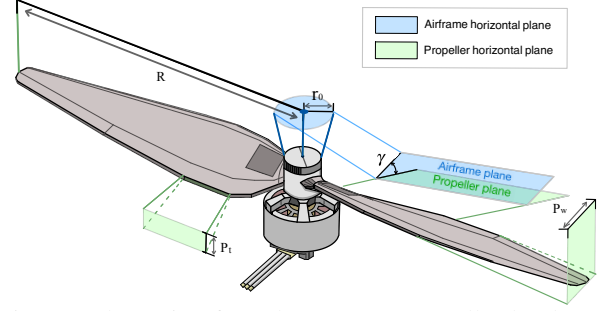


Fig. 3: Schematic of quadrotor UAV propeller hardware.

propeller radius R refers to the sum of the blade length r and the radius of the mounting interface r_0 . The blade mounting angle is the angle between the propeller blades and the plane of the UAV airframe, denoted by γ . Along with the blade width P_w , thickness P_t , we define the torque coefficient as,

$$C_M(t) = 2R \cdot C_T(t) = \frac{\left(\frac{1}{2\pi}\right)^2 \rho_a(t)(2R)^5}{N_B \int_{r_0}^R P_t^4 P_w Q_\gamma(t) dr}, \quad (5)$$

where N_B is the number of propeller blades, and $Q_\gamma(t)$ is determined by the propeller blade mounting angle and yaw angle in the current state. $\rho_a(t)$ is the air density determined by the atmospheric pressure at the location of the UAV and the absolute temperature, specifically,

$$\rho_a(t) = \frac{P_g \cdot M_g}{R_g \cdot T(t)}, \quad (6)$$

where P_g is the standard atmosphere, M_g is the molecular weight of gas, R_g is the gas constant, $T(t)$ is the outside ambient temperature, $z(t)$ is the height of flight at the location of the UAV, and M_g and R_g are constants in the ideal gas state.

The values of propeller radius R and airframe wheelbase $2l$ need to be set properly, in order to avoid collisions between neighboring propellers and underpowered situations. We illustrate the structural relationship in Fig. 4. In a symmetrically structured quadrotor configuration, the diagonal separation distance between neighboring propellers is $\sqrt{2}l$, and the total width of the two propellers ($2R$) must be less than this distance to avoid collision, namely $2R < \sqrt{2}l$. On the other hand, a too small R (less than $l/3$) will not provide enough lift for the UAV according to (3). Thus, there is a constrained relationship between R and l , namely $\frac{\sqrt{2}}{2}l \geq R \geq \frac{1}{3}l$.

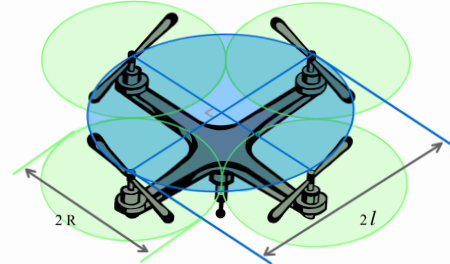


Fig. 4: Propeller radius in relationship to wheelbase for quadrotor UAV.

D. Transmission Rate

We define a tuple (m, n) to represent a transmission from m to n , where m and n can be $j \in \{1, 2, \dots, K\}$ (representing the j th MD), u (representing the UAV), or D (representing the DC).

We consider ζ_j to be a parameter determined by the carrier frequency f_c and obstacle density, corresponding to the proportion of the Line of Sight (LoS) path obstructed between the j th MD and the UAV, while the elevation angle of the link is θ_j . The probability to establish a LoS connection between the j th MD and the UAV is,

$$P_j^{\text{LoS}}(t) = \frac{1}{1 + \zeta_j \cdot \exp(-(\theta_j - \zeta_j))}. \quad (7)$$

The Signal-to-Interference-plus-Noise Ratio (SINR) for (m, n) at the t th timeslot is,

$$\xi_{(m,n)}(t) = \frac{p_j(t)}{L_{(m,n)}(t) \cdot (I_{(m,n)}(t) + \sigma_T^2)}, \quad (8)$$

where $p_j(t)$ is the transmission power of the j th MD at the t th timeslot. $L_{(m,n)}(t) = P_m^{\text{LoS}}(t) \cdot \left(\frac{4\pi f_c}{c} d_{(m,n)}(t)\right)^2$ is the path loss, c and $d_{(m,n)}(t)$ stand for the speed of light and the distance between m and n , respectively. $I_{(m,n)}(t)$ refers to the interference caused by concurrent transmissions, and σ_T^2 is the thermal noise.

We can then obtain the effective transmission rate for (m, n) at t th timeslot as,

$$r_{(m,n)}(t) = W_{(m,n)} \log_2(1 + \xi_{(m,n)}(t)), \quad (9)$$

where $W_{(m,n)}$ is the bandwidth of the wireless link.

E. Energy Consumption

We consider that the total energy consumption includes the consumption for the transmission and computation during the task offloading process, as well as those for the movement of the UAV. Hereafter, we use the binary variables $o_{ij}^{\text{MD}}(t)$, $o_{ij}^{\text{UAV}}(t)$, and $o_{ij}^{\text{DC}}(t)$ to specify the assignment of the i th task from the j th MD at the t th timeslot. A value of 1 indicates that the task is assigned to the corresponding location.

1) *UAV movement*: We consider that the motion state of the UAV is directly related to the rotational speed of the four DC motors. Thus, the energy consumption due to UAV movement at the t th timeslot is,

$$E^{\text{MOV}}(t) = \sum_{i=1}^4 (I_i(t) \cdot L) = \sum_{i=1}^4 \left(\frac{V_m - \omega_i(t) P_m}{R_m} \cdot L \right), \quad (10)$$

where $I_i(t)$ is the motor current, which can be calculated by (28) and (2) given that U and $\omega_i(t)$ ($i = 1, 2, 3, 4$) (the linear speed of i th motor rotation (r/min) at the t th timeslot) are obtained by our proposed attitude control method. V_m is the motor rated voltage, R_m is the rated resistance of the UAV motor circuit, and P_m is the electric potential constant determined by the motor structure.

2) *Energy consumption for transmission*: If a task is assigned to the UAV, two segments of transmission will be incurred, namely from the MD to the UAV and the UAV back to the MD. On the other hand, if a task is assigned to the DC, two additional segments, namely from the UAV to the DC and from the DC back to the UAV, will be incurred. Therefore, energy consumption at the t th timeslot for transmitting the i th task from the j th MD is,

$$e_{ij}^{\text{TR}}(t) = \left(o_{ij}^{\text{UAV}}(t) + o_{ij}^{\text{DC}}(t) \right) \left(\frac{p_j(t) s_{ij}(t)}{C_j(t) r_{(j,u)}(t)} + \frac{p_u(t) s_{ij}(t)}{C_j(t) r_{(u,j)}(t)} \right) + o_{ij}^{\text{DC}}(t) \left(\frac{p_u(t) s_{ij}(t)}{C_j(t) r_{(u,D)}(t)} + \frac{p_D(t) s_{ij}(t)}{C_j(t) r_{(D,u)}(t)} \right), \quad (11)$$

where $C_j(t)$ is the number of channels assigned to the j th MD.

3) *Energy consumption for computation*: We consider that the additional energy consumption for computing a finite number of tasks in the DC is negligible as the DC is assumed to be always active in processing tasks from different sources. Therefore, the energy consumption for computing i th task of the j th MD can be obtained by

$$e_{ij}^{\text{COMP}}(t) = o_{ij}^{\text{UAV}}(t) \delta_u s_{ij}(t) c_{ij}(f(t))^2 + o_{ij}^{\text{MD}}(t) \delta_j s_{ij}(t) c_{ij}(f_j(t))^2, \quad (12)$$

where δ_u and δ_j are the effective computing capacities of the UAV, and the j th MD, respectively.

4) *Overall Energy Consumption*: based on the discussions above, the overall energy consumption at the t th timeslot can be expressed as,

$$\mathbb{E}(t) = \sum_{j=1}^K \sum_{i=1}^{N_j} [e_{ij}^{\text{TR}}(t) + e_{ij}^{\text{COM}}(t)] + E^{\text{MOV}}(t), \quad (13)$$

where N_j is the total number of tasks for the j th UD.

F. Delay

We consider three delay components: transmission, computation, and queuing.

1) *Transmission delay*: the transmission delay for the i th task from the j th MD at the t th timeslot is,

$$d_{ij}^{\text{TR}}(t) = o_{ij}^{\text{DC}}(t) \left(\frac{s_{ij}(t)}{C_j(t) r_{(u,D)}(t)} + \frac{s_{ij}(t)}{C_j(t) r_{(D,u)}(t)} \right) + \left(o_{ij}^{\text{UAV}}(t) + o_{ij}^{\text{DC}}(t) \right) \left(\frac{s_{ij}(t)}{C_j(t) r_{(j,u)}(t)} + \frac{s_{ij}(t)}{C_j(t) r_{(u,j)}(t)} \right). \quad (14)$$

2) *Computation delay*: the delay for computing the i th task from the j th MD can be expressed as,

$$d_{ij}^{\text{COMP}}(t) = o_{ij}^{\text{UAV}}(t) \frac{s_{ij}(t) c_{ij}}{f(t)} + o_{ij}^{\text{MD}}(t) \frac{s_{ij}(t) c_{ij}}{f_j(t)}. \quad (15)$$

Note that as the computing resources at the DC are sufficient for all practical purposes, we assume that the computation delay at the DC is negligible.

3) *Queuing delay*: Consider that the arrival rate for transmission from the j th MD to UAV is λ_j , and the processing rate at the UAV for receiving transmissions is $[L \cdot C_j(t) \cdot r_{j,u}(t)]/s_j(t)$, where $s_j(t) = \sum_{i=1}^{N_j} s_{ij}(t)$ is the sum of tasks data size from that MD. If the total arrival rate is larger than the processing rate, a queuing delay for transmission will be incurred [14], that is,

$$d_{ij}^Q(t) = \frac{\lambda_j(1-p_j)s_j(t)^2}{L \cdot C_j(t)r_{j,u}(t) \cdot (L \cdot C_j(t)r_{j,u}(t) - \lambda_j(1-p_j)s_j(t))}. \quad (16)$$

Similarly, if the total sizes of arriving tasks exceed the computation capacity of the component, queuing delay for computation would be incurred for a proportion of the tasks. The expected queuing delay of the i th task from the j th MD executed at UAV at t th timeslot is,

$$d_{ij}^{\text{UAVQ}}(t) = \frac{\bar{Q}}{\sum_{j=1}^K \lambda_j(1-p_j)} - \frac{\sum_{j=1}^K \lambda_j(1-p_j)s_j(t)c_j}{\tau f(t) \sum_{j=1}^K \lambda_j(1-p_j)}, \quad (17)$$

where \bar{Q} is a parameter related to the computing capacity of the UAV.

4) *Total delay*: The total delay is obtained by summing all delay components mentioned earlier, that is,

$$\mathbb{D}(t) = \sum_{j=1}^K \sum_{i=1}^{N_j} (d_{ij}^{\text{TR}}(t) + d_{ij}^{\text{COMP}}(t) + d_{ij}^{\text{UAVQ}}(t) + d_{ij}^Q(t)). \quad (18)$$

IV. JOINT OPTIMIZATION PROBLEM

A. Attitude Control

1) *Classical PID Control*: The classical PID control algorithm is a widely used algorithm for UAV attitude control [19]. It considers the following three control parts:

- Proportional control (P): the error of the controller input is amplified by a certain proportion. This constitutes the basic control part;
- Integral control (I): an integral term is introduced for correction of the proportional control to maintain the system stability. Its coefficient will approach 0 as time goes by;
- Differential control (D): a differential term based on the rate of change of the input error is added. The purpose is to improve the response accuracy by predicting the future trend of the input error.

The classical PID control is described by the following equation,

$$U(t) = k_p e(t) + k_i \int e(t) dt + k_d \frac{d}{dt} e(t), \quad (19)$$

where k_p , k_i and k_d are the proportional, integral and differential coefficients, respectively. The output of the PID control system, $U(t)$, will affect $\omega, \theta, \phi, \psi$, which will in turns have an impact

on the power consumption of the UAV (see Section III-B and Appendix A for details).

2) *Fuzzy PID Control*: A major shortcoming of the classical PID control is that, as the coefficients k_p , k_i , and k_d are constants, it cannot adapt to dynamic environments and inter-dependent parameters as in UAV assisted fog computing scenarios. Therefore, we propose the fuzzy PID control algorithm, a nonlinear control technique with adaptive capability based on the Fuzzy set theory [20].

The fuzzy control process is demonstrated in Fig. 5. The key part of the process is the fuzzy controller at the top of Fig. 5), which determines Δk_p , Δk_i , and Δk_d , the adjustments in control coefficients, based on the yaw angle error E and the error rate EC from the previous estimation. The specific rules are shown in Table III. Based on the demand for Mamdani reasoning method in solving fuzzy PID problems [46], we establish the allowable value of E , EC , Δk_p , Δk_i , and Δk_d in Table IV.

TABLE III: FUZZY PID CONTROL RULES

| E | EC | | | | | |
|----|----------|----------|----------|----------|----------|----------|
| | NB | NM | NS | PS | PM | PB |
| NB | PB/NB/PS | PB/NB/NS | PM/NM/NB | PS/NS/NB | ZO/ZO/NM | ZO/ZO/PS |
| NM | PB/NB/PS | PB/NB/NS | PM/NM/NB | PS/NS/NM | ZO/ZO/NS | NS/PS/ZO |
| NS | PM/NB/ZO | PM/NM/NS | PM/NM/NS | ZO/ZO/NS | NS/PM/NS | NS/PM/ZO |
| ZO | PM/NM/ZO | PM/NM/NS | PS/NS/NS | ZO/ZO/NS | NS/PM/NS | NM/PM/ZO |
| PS | PS/NM/ZO | PS/NS/ZO | ZO/ZO/ZO | NS/PS/ZO | NM/PM/ZO | NM/PB/ZO |
| PM | PS/ZO/PB | ZO/ZO/PM | NS/PS/PM | NM/PS/PM | NM/PM/PS | NM/PB/PS |
| PB | ZO/ZO/PB | ZO/ZO/PM | NM/PS/PM | NM/PM/PM | NM/PM/PS | NB/PB/PS |

TABLE IV: FUZZY PID PARAMETER SETTINGS

| Parameters | Values | Parameters | Values | Parameters | Values |
|------------|---|--------------------------|------------------------|--------------|------------------------|
| E, EC | -6, -5, -4, -3, -2, -1, 0, 1, 2, 3, 4, 5, 6 | $\Delta k_p, \Delta k_d$ | -3, -2, -1, 0, 1, 2, 3 | Δk_i | -3, -2, -1, 0, 1, 2, 3 |

$$\begin{cases} k_{p-Fuzzy} = k_p + \Delta k_p \\ k_{i-Fuzzy} = k_i + \Delta k_i \\ k_{d-Fuzzy} = k_d + \Delta k_d. \end{cases} \quad (20)$$

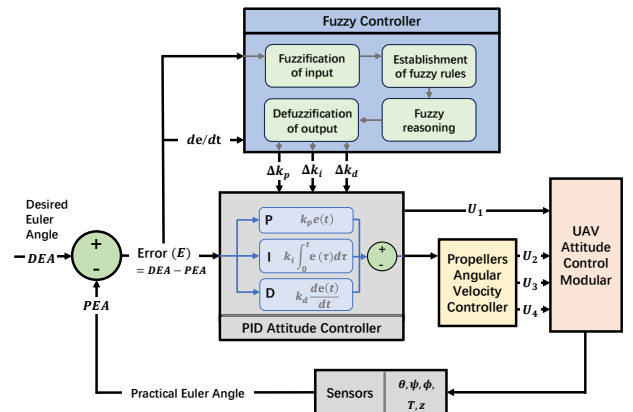


Fig. 5: Schematic structure of Fuzzy PID control system for quadrotor UAV.

B. Joint optimization model

We consider that the operational efficiency cost of the network is determined by the weighted sum of the energy and delay components. Therefore, our objective function consists of the energy consumption defined in (13) and the time required to complete all tasks defined in (18), during the entire period of T , as follows.

$$\begin{aligned}
& \text{Min} \\
& \{\mathbf{o}_{ij}(t), \mathbf{v}(t), \omega_i(t) | t \in \{0, \dots, T\}\} \\
& \text{s.t.} \\
& \mathbb{S} = \sum_{t=0}^T [\mathbb{D}(t) + \varepsilon \cdot \mathbb{E}(t)] \\
& (\mathbb{C}_1) \quad 0 \leq |\mathbf{v}(t)| \leq v^{\max} \\
& (\mathbb{C}_2) \quad 0 \leq z(t) \leq z^{\max} \\
& (\mathbb{C}_3) \quad \sum_{j=1}^K C_j(t) \leq N_c \\
& (\mathbb{C}_4) \quad f^{\min} \leq f(t) \leq f^{\max} \\
& (\mathbb{C}_5) \quad f_j^{\min} \leq f_j(t) \leq f_j^{\max} \\
& (\mathbb{C}_6) \quad p^{\min} \leq p(t) \leq p^{\max} \\
& (\mathbb{C}_7) \quad p_j^{\min} \leq p_j(t) \leq p_j^{\max} \\
& (\mathbb{C}_8) \quad o_{ij}^{\text{MD}}(t) + o_{ij}^{\text{UAV}}(t) + o_{ij}^{\text{DC}}(t) = 1 \\
& (\mathbb{C}_9) \quad o_{ij}^{\text{MD}}(t), o_{ij}^{\text{UAV}}(t), o_{ij}^{\text{DC}}(t) \in \{0, 1\} \\
& (\mathbb{C}_{10}) \quad \sum_{t=0}^T (E^{\text{UAV}}(t)) \leq B_c \\
& i \in \{1, \dots, N_j\}, j \in \{1, \dots, K\}
\end{aligned} \tag{21}$$

The decision variables include the angular velocities $\omega_i(t)$ related to attitude control, the velocity vector $\mathbf{v}(t)$ for trajectory planning, and task assignment decisions $\mathbf{o}_{ij}(t)$. The parameter ε is a weighting factor in the objective function, which flexibly caters to different magnitudes and ranges of the two measurements, as well as reflects the preference in terms of the trade-off between the two metrics in various fog computing scenarios. We will demonstrate in the result section that our proposed approach can achieve high performances for a wide range of ε values. In terms of the constraints, \mathbb{C}_1 to \mathbb{C}_3 were described in detail previously when they first appeared. \mathbb{C}_4 to \mathbb{C}_7 ensure that the processing frequency and transmission power of UAV and MDs are always within the effective range. \mathbb{C}_8 and \mathbb{C}_9 guarantee that every task is executed at exactly one place at any moment (no duplicate computing). \mathbb{C}_{10} restricts that the total energy consumption of the UAV during T does not exceed its battery capacity, as $E^{\text{UAV}}(t)$ denotes the energy consumption of the UAV at the t th timeslot,

$$\begin{aligned}
E^{\text{UAV}}(t) = & E^{\text{MOV}}(t) + \sum_{j=1}^K \sum_{i=1}^{N_j} \left[o_{ij}^{\text{DC}}(t) \left(\frac{p_u(t)s_{ij}(t)}{C_j(t)r_{(u,D)}(t)} \right) \right. \\
& \left. + o_{ij}^{\text{UAV}}(t) \left(\frac{p_u(t)s_{ij}(t)}{C_j(t)r_{(u,j)}(t)} + \delta_u s_{ij}(t) c_{ij}(f(t))^2 \right) \right].
\end{aligned} \tag{22}$$

Note that the processing frequencies $f(t)$, $f_j(t)$, and transmission powers $p(t)$, $p_j(t)$ are dependent on the decision variables $\mathbf{o}_{ij}(t)$. Numerous scholarly works provide comprehensive analyses of these intricate interactions, e.g., [14].

V. ALGORITHMS

The problem (21) possesses an intrinsic nonconvex nature. We divide the problem into two subproblems, one focusing on generating an initial trajectory and altitude, and the other on task assignment and resource allocation, as well as further tuning the trajectory. We propose two algorithms to address the two subproblems, respectively, with enhanced decoupling and safety values mechanism incorporated in the second algorithm to overcome the deadlock issue in conventional heuristic algorithms.

An overview of the steps in our proposed framework to address the joint optimization problem is shown in Fig. 6. We will apply an Ant Colony System based algorithm (Algorithm 2, to be described in detail later) to determine an initial trajectory based on the terrain of the area and the position of MDs. Then, the attitude control mechanism described in Section IV-A will be invoked to determine the as well as tune the trajectory. Finally, a Particle Swarm Optimization based algorithm (Algorithm 1, which was initially proposed in the conference version [15]) will determine the optimal task assignments and resource allocations. We will also analyze the convergence performance of the proposed algorithms at the end of the section.

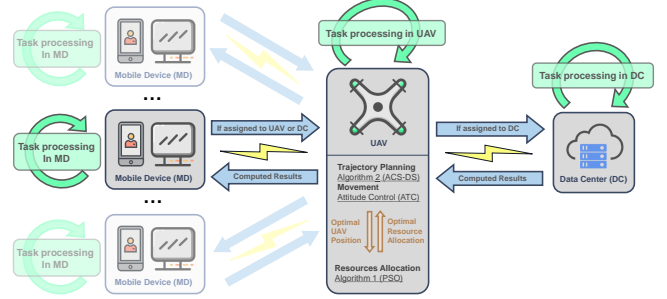


Fig. 6: A flowchart demonstration of the components in our proposed framework.

A. PSO for Task Assignment and Resource Allocation

We first introduce an algorithm based on the idea of Particle Swarm Optimization (PSO), for assigning tasks and allocating resources given that the trajectory is already known. The steps of our proposed algorithm are demonstrated in Algorithm 1, which we refer the readers to the conference version of this paper [15] for more detailed explanations. We categorize the job assignment decision, transmission power, and processing frequency as a collective entity $s_h = (\mathbf{o}_{ij}, p_j(t), f_j(t))$ within the particle swarm. Here, $h \in \{1, \dots, H\}$. Next, the determination of the particle group's position is carried out by uniformly sampling a set of particle groups denoted by $H \in \mathbb{N}_+$. In order to search for the optimal solution, the velocity of the particle groups is initialized and subsequently updated using the method in [47]. The algorithm terminates when the discrepancy between the outcomes of 20 successive rounds is less than a specified threshold δ , and then outputs the minimal value \mathbb{S}^* , the optimal decision for job assignment \mathbf{o}_{ij}^* , the transmission power $p_j^*(t)$, and the processing frequency $f_j^*(t)$.

B. ACS-DS for Trajectory Planning: Motivation and Concept

We now present the concept and outlines of the ACS-DS (ACS with **Decoupling** and **Safety values**) algorithm to generate the optimal UAV trajectory to minimize E^{MOV} . Then, we will prove that ACS-DS always converges to the optimal solution in polynomial time in subsequent subsections.

We first divide the 3D space into discrete grids, with the center of each unit of the grid serving as a *waypoint*, that is, the position that the UAV will pass. The 3D terrain is generated

Algorithm 1 Task Assignment, Power and Frequency Allocations based on Particle Swarm Optimization

Input: The length of an interval t , $p_j^{\max}(t)$; $p_j^{\min}(t)$; $f_j^{\max}(t)$; $f_j^{\min}(t)$; F_{A1} ; F_{A2} ; F_I

Output: $\mathbb{S}^*(t)$; \mathbf{o}_{ij}^* ; $p_j^*(t)$; $f_j^*(t)$

```

1: for  $h = 1$  to  $H$  do
2:   Initialize particles' position  $G_h$ 
3:   Initialize particles' velocity  $V_h$ 
4:   Initialize  $pBest_h \leftarrow G_h$ 
5:   Initialize  $gBest(0) \leftarrow \text{argmin}_{fit}(pBest_h)$ , where  $fit$  represent the equation to compute  $\mathbb{S}^*(t)$ ;  $k = 1$ 
6:   for  $h = 1$  to  $H$  do
7:     Update  $V_h$  and  $G_h$  by acceleration factors  $F_{A1}$ ,  $F_{A2}$  and  $F_I$ 
8:     if  $fit(G_h) < fit(pBest_h)$  then
9:        $pBest_h \leftarrow G_h$ 
10:    if  $fit(pBest_h) < fit(gBest)$  then
11:       $gBest(k) \leftarrow pBest_h$ 
12:     $k \leftarrow (k + 1)$ 
13:  while  $|gBest(k + 1) - gBest(k)| < \delta$  do
14:     $\mathbb{S}^*(t) \leftarrow fit(gBest)$ 
15:     $(\mathbf{o}_{ij}^*; p_j^*(t); f_j^*(t)) \leftarrow gBest$ 
16:  Output  $\mathbb{S}^*(t)$ ;  $(\mathbf{o}_{ij}^*; p_j^*(t); f_j^*(t))$ 

```

randomly, and we denote the area at and below terrain surfaces, referred as the *no-fly zone*, by $O = \{(x_n^o, y_n^o, z_n^o)\}$, where $n \in \{1, 2, \dots, N_o\}$, and N_o is the total number of grids in the no-fly zone. Note that the classical ACS is not applicable to our three-dimensional trajectory planning problem as it struggles to converge in path searching in large three-dimensional spaces, and is likely to be trapped in local optima.

To overcome these issues and obtain the optimal trajectory with minimum cost in an efficient manner, we propose the ACS-DS, by incorporate the two special mechanisms to the classical ACS. We now elaborate these two mechanisms.

1) *Safety Values*: We enhance the heuristic function of the ACS-DS by adding a security value at each step based on the number of currently known the numbers of feasible and infeasible waypoints. Specifically, we determine the safety value of a waypoint based on the proportion of known feasible waypoints in the next available position for that waypoint. The safety value from waypoint μ to ν is calculated as $\kappa_{\mu\nu} = \frac{N_f - N_{\mu\nu}}{N_f}$, where N_f denotes the total number of waypoints in a preset constant range $[0, R_f]$, and $N_{\mu\nu}$ denotes the number of infeasible waypoints in the range of N_f over direction from μ to ν . Safety values are updated using a similar rule to pheromones, and when choosing its next move, the ant would add the safety values to the pheromone levels for all possible actions. We will show in the results section that this method can reduce the running time and improve the operation efficiency compare to the classical ACS algorithm.

2) *Decoupling*: In ACS, when an ant reaches a point with no further viable options, it becomes trapped in a deadlock. To

address this issue, we introduce a mechanism that allows the ant to escape the deadlock. Specifically, when any of following rule is satisfied during the ant's movement, the Decoupling mechanism will be triggered to perform a backtracking behavior with depth (step size) D_b to find alternative directions:

- An ant repeats a closed cycle consisting of two or more waypoints over multiple consecutive timeslots.
- A sudden drop in the amount of pheromone and safety values occurs, as indicated by the fact that the κ of the currently selected waypoint is less than half that of the previous waypoint.
- An ant falls into a local optimum and undetected in the early stage, that is, the ant has not triggered backtracking behavior for more than 25 consecutive waypoints in the first one-third of all iterations.

It is worth noting that the third rule is only considered in the early stages of the algorithm (first one-third of all iterations) to avoid excessive backtracking that reduces the convergence speed of the algorithm. This mechanism, by dynamically adjusting the pheromone levels and allowing the ant to backtrack and explore new possibilities, ensures that the ACS-DS remains robust and capable of finding optimal trajectories even in complex and challenging scenarios.

C. ACS-DS: Detailed Steps

We let m be the total number of ants in the colony, and $\sigma = V_p + \kappa$ be the guidance factor. We further denote $\sigma_{\mu\nu}(h)$ as the sum of pheromone values and safety values between the neighboring waypoints μ and ν in the h th iteration. The initial pheromones on each edge are equal, namely $\sigma_{\mu\nu}(0) = C$ for all μ and ν . We denote by s^* the global best path obtained by the algorithm, corresponding to the minimal-cost trajectory in our UAV optimization problem. Next, for each ant $k \in \{1, 2, \dots, m\}$ in the colony, we initialize the pheromone V_{p0} , the safety value κ_0 , and the heuristic value η . We also define the evaporation rate $\rho \in (0, 1)$ representing the degree to which the guidance factor $\sigma_{\mu\nu}(h)$ decays with iterations. Finally, we define S_t as the set of waypoints that ant t can pass next, and $p_{\mu\nu}^t(h)$ as the probability that ant t moves from position μ to ν in the h th iteration. The exact value of $p_{\mu\nu}^t(h)$ is jointly determined by the guidance factor and heuristic value at the waypoint, as in the following equation,

$$p_{\mu\nu}^t(h) = \begin{cases} \frac{\sigma_{\mu\nu}^{\alpha}(h) \eta_{\mu\nu}^{\beta}(h)}{\sum_{r \in S_t} \sigma_{\mu r}^{\alpha} \eta_{\mu r}^{\beta}(h)} & \nu \in S_t, \\ 0 & \text{otherwise.} \end{cases} \quad (23)$$

Detailed steps of ACS-DS are presented in Algorithm 2.

D. ACS-DS: Proof of convergence

We now prove that Algorithm 2 will eventually converge, starting by the following proposition.

Proposition 1. *In Algorithm 2, for the guidance factor $\sigma_{\mu\nu}$ on any edge (μ, ν) generated by the ants during the searching process, there exists a maximum value $g(s^*)$ as $h \rightarrow \infty$.*

Algorithm 2 ACS-DS: ACS-based Trajectory Planning with Decoupling and Safety Values Mechanisms

Input: Positions of all MDs (x_j, y_j, z_j) ; ρ ; η ; V_{P0} ; κ_0 ; terrain surface with no-fly zone $(x_n^o, y_n^o, z_n^o) \in O$

Output: $E^{\text{MOV}^*}(t)$; Trajectory of the UAV $(x_t(t), y_t(t), z_t(t))$

```

1: for  $h = 1$  to  $H$  do
2:   Randomly set the initial coordinate of the UAV,
    $(x(0), y(0), z(0))$ 
3:   while  $(x(0), y(0), z(0)) \notin O$  do
4:     for each edge do
5:       Set initial pheromone, and calculate the initial
       safety values
6:       for each ant  $\iota$  do
7:          $(x_\iota(h), y_\iota(h), z_\iota(h)) = (x(0), y(0), z(0))$ 
8:         for each edge  $(\mu, \nu)$  do
9:           Choose the next coordinate with probability
            $p_{\mu\nu}^l(h)$  by  $\sigma$  and  $\eta$ 
10:          while  $(x_\iota(h+1), y_\iota(h+1), z_\iota(h+1)) \notin O$  do
11:            Output  $(x_\iota(h+1), y_\iota(h+1), z_\iota(h+1))$ 
12:          Compute and output the length  $\sum_{t=1}^T d_u(t)$  of
          the path by the  $\iota$ th ant and  $E_u$ 
13:          for each edge  $(\mu, \nu)$  do
14:            Update  $V_{P_{\mu\nu}}$  and  $\kappa_{\mu\nu}$  by  $\rho$ 
15:            Update  $\sigma_{\mu\nu}(h)$  by  $V_{P_{\mu\nu}}$  and  $\kappa_{\mu\nu}$ 
16: Compute and output  $E^{\text{MOV}^*}(t)$  by (10).
```

Proof. For ACS-DS, the local update of the guidance factor for edge (μ, ν) after the completion of each round of iteration can be represented as $\sigma_{\mu\nu}(h+1) = (1 - \phi) \cdot \sigma_{\mu\nu}(h) + \phi \cdot \Delta\sigma_{\mu\nu}(h)$, while the global guidance factor is updated in a similar way, that is, $\sigma(h+1) = (1 - \phi) \cdot \sigma(h) + \phi \cdot \Delta\sigma(h)$. Here, $\Delta\sigma_{\mu\nu}(h) = \sigma_{\mu\nu}(h) - \sigma_{\mu\nu}(h-1)$ is the increment of guidance factor on edge (μ, ν) at the h th iteration.

$$\begin{aligned}
\sigma_{\mu\nu}(1) &= (1 - \phi) \cdot \sigma_{\mu\nu}(0) + \phi \cdot \Delta\sigma_{\mu\nu}(0) \\
&\dots \\
\sigma_{\mu\nu}(h) &= (1 - \phi)^h \cdot \sigma_{\mu\nu}(0) + (1 - \phi)^{h-1} \cdot \phi \cdot \Delta\sigma_{\mu\nu}(1) + \dots \\
&\quad + (1 - \phi) \cdot \phi \cdot \Delta\sigma_{\mu\nu}(h-1) + \phi \cdot \Delta\sigma_{\mu\nu}(h) \\
&= \sum_{q=1}^h \left((1 - \phi)^{h-q} \cdot \phi \cdot \Delta\sigma_{\mu\nu}(q) + (1 - \phi)^h \cdot \sigma_{\mu\nu}(0) \right) \\
\lim_{h \rightarrow \infty} \sigma_{\mu\nu}^{\max}(h) &= \lim_{h \rightarrow \infty} \left(\sum_{q=1}^h \left((1 - \phi)^{h-q} \cdot \phi \cdot \Delta\sigma_{\mu\nu}(q) + \dots \right) \right) \\
&= g(s^*) < \infty.
\end{aligned} \tag{24}$$

Thus, the guidance factor on each edge is bounded from the above by $g(s^*)$. \square

After the first optimal solution is found, the guidance factor on the elements belonging to an optimal solution is guaranteed to be no less than that on other elements as we have a sufficient number of subsequent generations. That is, the guidance factor

on any element not belonging to an optimal solution will keep decreasing until it is no larger than the guidance factor on the elements belonging to an optimal solution. In mathematical terms, we have the following corollary.

Corollary 1. As $h \rightarrow \infty$, it is always true that $\sigma_{\mu\nu}(h) \geq \sigma_{\mu'\nu'}(h)$, if $(\mu, \nu) \in s^*$ and $(\mu', \nu') \notin s^*$.

Proof. Suppose it takes h^* generations to find the first optimal solution. We assume that for a certain $(\mu, \nu) \in s^*$, there exists a $(\mu', \nu') \notin s^*$, $\sigma_{\mu\nu}(h^*) < \sigma_{\mu'\nu'}(h^*)$. Then, based on the guidance factor update rule in ACS-DS, by the $h^* + h'$ generation, the guidance factor on (μ', ν') can be derived as

$$\sigma_{\mu'\nu'}(h^* + h') = \max \left\{ \sigma_{\mu\nu}(h^*), (1 - \rho)^{h'} \cdot \sigma_{\mu'\nu'}(h^*) \right\} \tag{25}$$

Therefore,

$$\begin{aligned}
\lim_{h \rightarrow \infty} \sigma_{\mu'\nu'}(h^* + h') &= \max \lim_{h \rightarrow \infty} \left\{ \sigma_{\mu\nu}(h^*), [(1 - \rho)^{h'} \cdot \sigma_{\mu'\nu'}(h^*)] \right\} \\
&= \max \left\{ \sigma_{\mu\nu}(h^*), 0 \right\} \\
&\leq \sigma_{\mu\nu}(h^*)
\end{aligned} \tag{26}$$

\square

Proposition 1 and Corollary 1 jointly prove that, after a sufficient number of iterations, the guidance factor on an optimal path is bounded and no less than those on other paths. Noticeably, the backtracking behavior caused by the decoupling mechanism in ACS-DS will only increase the number of iterations for the current waypoint, but does not affect the updating of the guidance factor and the convergence to the optimal solution as in the original ACS. Therefore, the ACS-DS algorithm always converges to the global optimal solution.

E. ACS-DS: Complexity analysis

We now analyze the complexity of Algorithm 2 when a total of n users initiate computation requests in the current timeslot. Assume that in the worst case, Algorithm 2 triggers backtracking at every waypoint for each ant upfront, the path construction time complexity for m ants is $O(m \cdot n^2)$. The complexity of each update of the guidance factor, and each calculation of the transfer probability is $O(n^2)$. If the algorithm is finished after H iterations, the complexity of the entire algorithm is $O(H \cdot m \cdot n^2 + H \cdot n^2)$. Since the magnitude of m is similar to n , the complexity of the ACS-DS algorithm in completing all the tasks of the network is approximately $O(H \cdot n^3)$, which means that Algorithm 2 has a polynomial time complexity.

VI. PERFORMANCE EVALUATION

In this section, we present numerical results of simulations on systems with various settings to assess the efficacy and versatility of our proposed solutions.

A. Experiment setup

We consider a three-dimensional spatial domain with dimensions of $S \times S \times Z$. K MDs are uniformly and randomly distributed in the space. Values of key system parameters are listed in Table V.

TABLE V: Values of relevant system parameters in the experiments

| Parameter | Value | Parameter | Value |
|------------|--|------------|--|
| S | 50000 m | Z | 3000 m |
| L | 0.1 s | ϵ | [0.05, 1.00] |
| m | 80 kg | a | 5.28 m/s ² |
| g | 9.81 m/s ² | l | 1150 mm |
| K | 50 | R | 512 mm |
| N_c | 40 | P_l | 7.5 mm |
| N_B | 2 | P_w | 250 mm |
| B_c | 5000 Wh | I_x | 0.095 |
| v_{\max} | 50 m/s | I_y | 0.095 |
| z_{\max} | 2500 m | I_z | 0.187 |
| C_T | 1.483 (N · m · min ²) / r ² | C_M | 2.925 (N · m · min ²) / r ² |
| M_g | 29 g/mol | R_g | 8.314 J/(mol · K) |

The values of parameters used in the algorithms described earlier in this paper are listed in Table VI. All experimental results presented in this section are based on the average of the 50 independent runs with the weighting factor ϵ randomly generated randomly within its domain for each run.

TABLE VI: Values of relevant algorithmic parameters

| Parameter | Value | Parameter | Value | Parameter | Value |
|------------------|-------|-----------|-------|------------|-------|
| ρ | 0.25 | V_{P0} | 3.8 | η | 2.5 |
| F_{A1}, F_{A2} | 2.0 | F_l | 0.65 | R_f, D_b | 200 m |

For the task assignment and resource allocation part, we adopt PSO (Algorithm 1), which has been demonstrated effective and robust in our earlier conference paper [15]), for all experiments in this section. For the attitude control and trajectory planning modules, we focus on evaluating the performance of our proposed ACS-DS (Algorithm 2) and ATC (Section IV-A). Specifically, we examine the following eight implementations and compare their performances in terms of overall operational efficiency cost.

- RAN: All tasks are randomly assigned to the MD, the UAV, or the data center. The channels, processing frequencies and power allocations are generated randomly in their respective domains. No special mechanisms are applied for attitude control or trajectory planning.
- PSO: The PSO algorithm (Algorithm 1) is used to determine task assignments, the processing frequencies, and transmission powers of MDs and the UAV. Allocation of channels in accordance with the methodology described in Section III. No special mechanisms are applied for attitude control or trajectory planning.
- ACS: On top of PSO, trajectory of the UAV is planned by the classical ACS.
- ACS + ATC: On top of ACS, the mechanism described in Section IV-A is added to control the attitude of the UAV.
- ACS-D: On top of PSO, trajectory of the UAV is planned by ACS with the decoupling mechanism.
- ACS-D + ATC: The mechanism described in Section IV-A is added to control the attitude of the UAV on top of ACS-D.

- ACS-DS: On top of PSO. Trajectory of the UAV is planned by ACS with decoupling and safety values mechanisms in Algorithm 2.
- ACS-DS + ATC: The mechanism described in Section IV-A is added to control the attitude of the UAV on top of ACS-DS.

B. Numerical results

1) *Optimal Propeller Parameters:* Fig. 7 shows the relationship between the overall energy consumption and propeller blade parameters including the number of blades, and the radius, width, mounting angle, and thickness of each blade, given that all other parameters are fixed. From the results, we can infer that, for a symmetric quadrotor UAV with a total mass of 80 kg, four rotors and a maximum acceleration up to 5.28 m/s², it is optimal to equip 2 propeller blades with a radius of 500 mm, a width of 250 mm and a thickness of 7.5 mm. The average energy consumption under configurations with optimal values of parameters can be reduced by more than 30%, compared to the average amount of 50 sets of random parameters generated uniformly within the respective allowable range of each parameter.

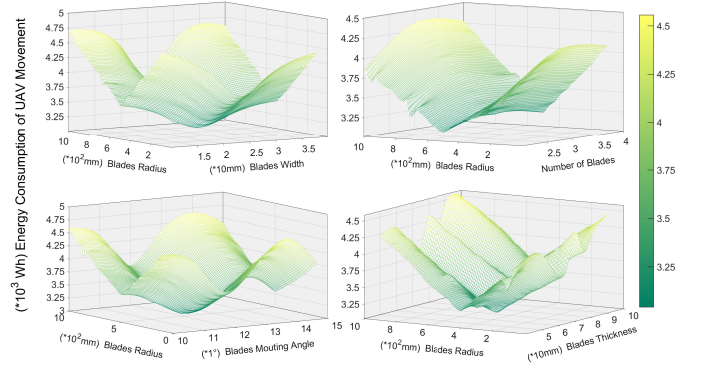


Fig. 7: Relationship between overall energy consumption and propeller blades parameters.

2) *Convergence Speed of Algorithms:* Fig. 8 demonstrates the average convergence speeds of 200 independent runs by the classical ACS, ACS-D and ACS-DS over 80 iterations. Both mechanisms, decoupling and safety values, reduce the energy consumption of UAV movement to an extent. In addition, with classical ACS as the baseline, ACS-D improves the convergence speed to obtain the optimal trajectory by more than 7%, while the improvement by ACS-DS is more than 15%.

3) *Trajectory planning:* We now generate the terrain height randomly as a continuous surface (no-fly zone) within the three-dimensional spatial domain as shown in Figs. 9 and 10, and consider that the MDs are placed directly on the ground conforming to the terrain height, in order to test the obstacle avoidance capability of our proposed trajectory planning and attitude control algorithms. We observe from the trajectories of the UAV in Figs. 9 and 10 that, both the additional mechanisms of decoupling and safety values in ACS and attitude control

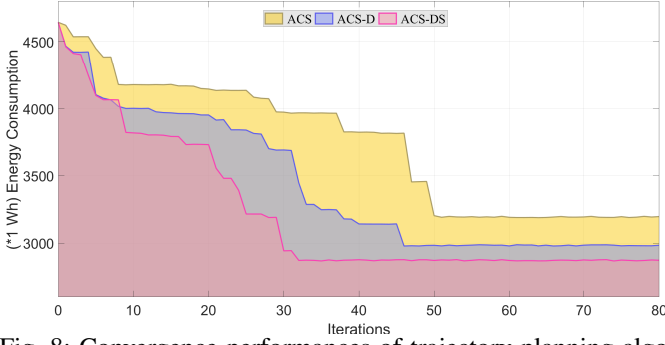


Fig. 8: Convergence performances of trajectory planning algorithms.

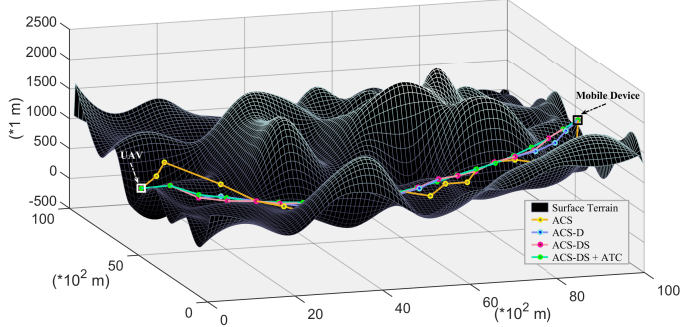


Fig. 9: A demonstration of trajectories planned by different mechanisms on a 3D spatial domain with terrain height generated randomly as a continuous surface.

(ATC) have positive impacts on the final path. Specifically, ATC achieves more stable and precise flight control by optimizing the UAV rotor speed in real time based on the feedback of error and environmental information from the sensors. By jointly applying the ACS with the decoupling, safety values and attitude control, ACS-DS+ATC obtains the smoothest and shortest trajectory among all.

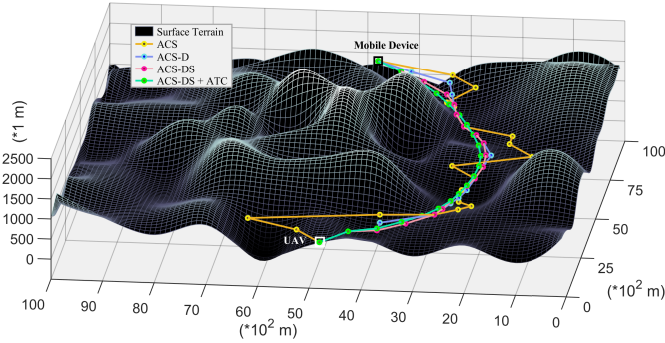


Fig. 10: Demonstration of trajectories planned by different mechanisms on a 3D spatial domain with terrain height generated randomly as a continuous surface (TOP).

4) *Operational Efficiency Cost*: Finally, we present the results of the operational efficiency cost (combining delay and energy consumption) achieved by the eight implementations in Fig. 11. Again, we can observe that the decoupling mechanism and safety values in ACS-DS can significantly reduce the overall consumption compared to the classical ACS.

In addition, our proposed attitude control mechanism (ATC)

can further improve the performance, irrespective of whether ACS, ACS-D, or ACS-DS is employed. Overall, ACS-DS+ATC can reduce the operational efficiency cost by more than 58% and 35% compared to RAN and classical ACS, respectively.

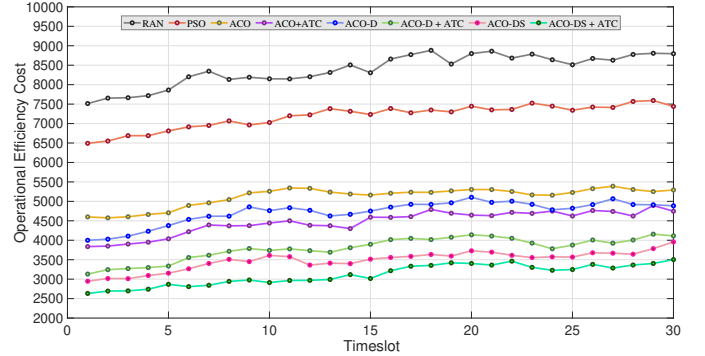


Fig. 11: Comparison of operational efficiency cost by different methods.

VII. CONCLUSIONS

In this paper, we have proposed a joint optimization framework to reduce the operational efficiency cost in UAV-assisted fog computing systems. Our proposed framework involves multiple modules, including quadrotor UAV attitude control, trajectory planning in a three-dimensional spatial domain with continuously varying terrain heights, and energy-efficient assignment of computing tasks to different components in the network. We have designed appropriate mechanisms or algorithms for each module in the framework, and integrated them together to obtain a holistic solution to improve the overall efficiency in UAV-assisted fog computing. Specifically, we have proposed a novel fuzzy PID control mechanism for effective attitude control, designed the ACS-DS algorithm that overcomes the convergence issue in conventional approaches for trajectory planning in three-dimensional domains, and a modified PSO algorithm to determine the optimal task assignment. Numerical results from a wide range of experiments have shown that our proposed framework can reduce the operational efficiency cost by over 35% compared to existing approaches.

APPENDIX

A. The Dynamics of a Quadrotor UAV

We consider two key components in the structure of a quadrotor UAV, namely the body frame and the earth frame. The body frame is commonly used for attitude control of the UAV, where the positive direction is the direction of ascent corresponding to the centers of the four motors.

We assume that the airframe has the following characteristics and constraints,

- The structure of the quadrotor UAV is symmetric;
- Friction between propeller and motor spindle is negligible;
- The stator magnetic field speed and rotor speed of the motors are infinitely close to each other, such that the slip rate is 0;

- The quadrotor and propeller structures are rigid, with a uniform mass distribution and the geometric center is the mass center;
- The Euler angles are bounded, i.e., $-\pi/2 < \phi < \pi/2, -\pi/2 < \theta < \pi/2, -\pi < \psi < \pi$.

Based on the above assumptions, we combine the dynamics principles to establish a rigid body model for attitude control of quadrotor UAV. It should be noted that all UAV coordinate system transformations are obtained by rotation synthesis with respect to the fixed coordinate system, the rotation matrix for the conversion of the body frame to the earth frame with the following equation,

$$R_e^b = (R_e^b)^{-1} = (R_e^b)^T = \begin{bmatrix} \cos \theta \cos \psi & \sin \theta \cos \psi \sin \phi & \sin \theta \cos \psi \sin \phi \\ \cos \theta \sin \psi & \sin \theta \sin \psi \sin \phi & \sin \theta \sin \psi \sin \phi \\ -\sin \theta & +\cos \psi \cos \phi & -\cos \psi \cos \phi \\ \cos \theta \sin \phi & \cos \theta \cos \phi & \cos \theta \cos \phi \end{bmatrix} \quad (27)$$

Four inputs, including pitch control quantity U_1 , roll control quantity U_2 , yaw control quantity U_3 , and altitude control quantity U_4 , can be controlled based on the torque of the four motors of the UAV, that is,

$$\begin{cases} U_1(t) = C_T(t) (\omega_1(t)^2 + \omega_2(t)^2 + \omega_3(t)^2 + \omega_4(t)^2) \\ U_2(t) = C_T(t) (-\omega_2(t)^2 + \omega_4(t)^2) \\ U_3(t) = C_T(t) (-\omega_1(t)^2 + \omega_3(t)^2) \\ U_4(t) = C_M(t) (-\omega_1(t)^2 + \omega_2(t)^2 - \omega_3(t)^2 + \omega_4(t)^2) \end{cases} \quad (28)$$

REFERENCES

- [1] K. Ashton, "That 'Internet of Things' thing," *RFiD Journal*, vol. 22, no. 7, pp. 97–114, 1999.
- [2] N. Hu, Z. Tian, X. Du, N. Guizani, and Z. Zhu, "Deep-green: A dispersed energy-efficiency computing paradigm for green industrial IoT," *IEEE Transactions on Green Communications and Networking*, vol. 5, no. 2, pp. 750–764, 2021.
- [3] S. Sarkar, S. Chatterjee, and S. Misra, "Assessment of the suitability of fog computing in the context of Internet of Things," *IEEE Transactions on Cloud Computing*, vol. 6, no. 1, pp. 46–59, 2018.
- [4] O. Ghdiri, W. Jaafar, S. Alfattani, J. B. Abderrazak, and H. Yanikomeroglu, "Offline and online UAV-enabled data collection in time-constrained IoT networks," *IEEE Transactions on Green Communications and Networking*, vol. 5, no. 4, pp. 1918–1933, 2021.
- [5] H. El Hammouti, M. Benjillali, B. Shihada, and M.-S. Alouini, "Learn-As-You-Fly: A distributed algorithm for joint 3D placement and user association in multi-UAVs networks," *IEEE Transaction Wireless Communication*, vol. 18, no. 12, pp. 5831–5844, 2019.
- [6] X. Wu and Y. Liu, "Trajectory tracking control of quadrotor UAV," in *2018 37th Chinese Control Conference (CCC)*, 2018, pp. 10020–10025.
- [7] Z. Ma and S. M. Jiao, "Research on the attitude control of quad-rotor UAV based on active disturbance rejection control," in *2017 3rd IEEE International Conference on Control Science and Systems Engineering (ICCSSE)*, 2017, pp. 45–49.
- [8] Z. Song, Y. Wang, L. Liu, Z. Cheng, and Y. Yang, "Research on attitude control of quadrotor UAV based on active disturbance rejection control," in *2020 Chinese Control And Decision Conference (CCDC)*, 2020, pp. 5051–5056.
- [9] Z. Kuang, H. Wang, J. Li, and F. Hou, "Utility-aware UAV deployment and task offloading in multi-UAV edge computing networks," *IEEE Internet of Things Journal*, vol. 11, no. 8, pp. 14755–14770, 2024.
- [10] M. Zhao, W. Li, L. Bao, J. Luo, Z. He, and D. Liu, "Fairness-aware task scheduling and resource allocation in UAV-enabled mobile edge computing networks," *IEEE Transactions on Green Communications and Networking*, vol. 5, no. 4, pp. 2174–2187, 2021.
- [11] K. Xiong, Y. Liu, L. Zhang, B. Gao, J. Cao, P. Fan, and K. B. Letaief, "Joint optimization of trajectory, task offloading, and CPU control in UAV-assisted wireless powered fog computing networks," *IEEE Transactions on Green Communications and Networking*, vol. 6, no. 3, pp. 1833–1845, 2022.
- [12] P. Poksawat, L. Wang, and A. Mohamed, "Gain scheduled attitude control of fixed-wing UAV with automatic controller tuning," *IEEE Transactions on Control Systems Technology*, vol. 26, no. 4, pp. 1192–1203, 2018.
- [13] E. Besada-Portas, L. de la Torre, J. M. de la Cruz, and B. de Andrés-Toro, "Evolutionary trajectory planner for multiple UAVs in realistic scenarios," *IEEE Transactions on Robotics*, vol. 26, no. 4, pp. 619–634, 2010.
- [14] X. Wei, C. Tang, J. Fan, and S. Subramaniam, "Joint optimization of energy consumption and delay in cloud-to-thing continuum," *IEEE Internet of Things Journal*, vol. 6, no. 2, pp. 2325–2337, 2019.
- [15] S. Liu, J. Yin, Z. Zeng, and J. Wu, "Optimal trajectory planning and task assignment for UAV-assisted fog computing," in *2022 IEEE 24th International Conference on High Performance Computing & Communications (HPCC)*, 2022, pp. 1400–1407.
- [16] E. Zhu, J. Pang, N. Sun, H. Gao, Q. Sun, and Z. Chen, "Airship horizontal trajectory tracking control based on active disturbance rejection control (ADRC)," *Nonlinear Dynamics*, vol. 75, pp. 725–734, 2014.
- [17] Y. He, Y. Gan, H. Cui, and M. Guizani, "Fairness-based 3-D multi-UAV trajectory optimization in multi-UAV-assisted MEC system," *IEEE Internet of Things Journal*, vol. 10, no. 13, pp. 11383–11395, 2023.
- [18] X. Huang, W. Luo, and J. Liu, "Attitude control of fixed-wing UAV based on DDQN," in *2019 Chinese Automation Congress (CAC)*, 2019, pp. 4722–4726.
- [19] K. C. U. Obias, M. F. Q. Say, E. A. V. Fernandez, A. Y. Chua, and E. Sybingco, "A study of the interaction of proportional-integral-derivative (PID) control in a quadcopter unmanned aerial vehicle (UAV) using design of experiment," in *2019 IEEE 11th International Conference on Humanoid, Nanotechnology, Information Technology, Communication and Control, Environment, and Management (HNICEM)*, 2019, pp. 1–4.
- [20] B. E. Demir, R. Bayir, and F. Duran, "Real-time trajectory tracking of an unmanned aerial vehicle using a self-tuning fuzzy proportional integral derivative controller," *International Journal of Micro Air Vehicles*, vol. 8, no. 4, pp. 252–268, 2016.
- [21] L. Shen, N. Wang, D. Zhang, J. Chen, X. Mu, and K. M. Wong, "Energy-aware dynamic trajectory planning for UAV-enabled data collection in mMTC networks," *IEEE Transactions on Green Communications and Networking*, vol. 6, no. 4, pp. 1957–1971, 2022.
- [22] M. Diallo, A. Quintero, and S. Pierre, "An efficient approach based on ant colony optimization and tabu search for a resource embedding across multiple cloud providers," *IEEE Transactions on Cloud Computing*, vol. 9, no. 3, pp. 896–909, 2019.
- [23] K. Dev, P. K. R. Maddikunta, T. R. Gadekallu, S. Bhattacharya, P. Hegde, and S. Singh, "Energy optimization for green communication in IoT using Harris Hawks Optimization," *IEEE Transactions on Green Communications and Networking*, vol. 6, no. 2, pp. 685–694, 2022.
- [24] X. He, K. Wang, H. Huang, T. Miyazaki, Y. Wang, and S. Guo, "Green resource allocation based on deep reinforcement learning in content-centric IoT," *IEEE Transactions on Emerging Topics in Computing*, vol. 8, no. 3, pp. 781–796, 2020.
- [25] R. Battiti and P. Campigotto, "An investigation of reinforcement learning for reactive search optimization," in *Autonomous Search*. Springer, 2012, pp. 131–160.
- [26] Y. Tao, J. Qiu, and S. Lai, "A hybrid cloud and edge control strategy for demand responses using deep reinforcement learning and transfer learning," *IEEE Transactions on Cloud Computing*, vol. 10, no. 1, pp. 56–71, 2021.
- [27] M. Jain, V. Saijpal, N. Singh, and S. B. Singh, "An overview of variants and advancements of PSO algorithm," *Applied Sciences*, vol. 12, no. 17, p. 8392, 2022.
- [28] J.-J. Shin and H. Bang, "UAV path planning under dynamic threats using an improved PSO algorithm," *International Journal of Aerospace Engineering*, vol. 2020, pp. 1–17, 2020.
- [29] M. Dorigo, G. Di Caro, and L. M. Gambardella, "Ant algorithms for discrete optimization," *Artificial life*, vol. 5, no. 2, pp. 137–172, 1999.
- [30] K. Socha, "ACO for continuous and mixed-variable optimization," in

International Workshop on Ant Colony Optimization and Swarm Intelligence, 2004, pp. 25–36.

- [31] Z. A. Ali, H. Zhangang, and W. B. Hang, “Cooperative path planning of multiple UAVs by using max–min ant colony optimization along with cauchy mutant operator,” *Fluctuation and Noise Letters*, vol. 20, no. 01, p. 2150002, 2021.
- [32] C. Wang, Y. Nan, S. Zhang, and L. Jiang, “Application of the adaptive double-layer ant colony algorithm in UAV trajectory planning,” in *2021 4th International Conference on Intelligent Autonomous Systems (ICoIAS)*, 2021, pp. 371–377.
- [33] D. Liu and S. Ji, “Research on efficient online planning of emergency logistics path based on double-layer ant colony optimization algorithm,” *International Journal of Computers and Applications*, vol. 41, no. 5, pp. 400–406, 2019.
- [34] J. Cui, Y. Liu, and A. Nallanathan, “Multi-agent reinforcement learning-based resource allocation for UAV networks,” *IEEE Transactions on Wireless Communications*, vol. 19, no. 2, pp. 729–743, 2019.
- [35] M. Li, N. Cheng, J. Gao, Y. Wang, L. Zhao, and X. Shen, “Energy-efficient UAV-assisted mobile edge computing: Resource allocation and trajectory optimization,” *IEEE Transactions on Vehicular Technology*, vol. 69, no. 3, pp. 3424–3438, 2020.
- [36] G. Wu, H. Wang, H. Zhang, Y. Zhao, S. Yu, and S. Shen, “Computation offloading method using stochastic games for software-defined-network-based multiagent mobile edge computing,” *IEEE Internet of Things Journal*, vol. 10, no. 20, pp. 17 620–17 634, 2023.
- [37] A. Lipare, D. R. Edla, and R. Dharavath, “Fuzzy rule generation using modified PSO for clustering in wireless sensor networks,” *IEEE Transactions on Green Communications and Networking*, vol. 5, no. 2, pp. 846–857, 2021.
- [38] Z. Zhou, Y. Nie, and G. Min, “Enhanced ant colony optimization algorithm for global path planning of mobile robots,” in *2013 International Conference on Computational and Information Sciences*, 2013, pp. 698–701.
- [39] W. Hou, Z. Xiong, C. Wang, and H. Chen, “Enhanced ant colony algorithm with communication mechanism for mobile robot path planning,” *Robotics and Autonomous Systems*, vol. 148, p. 103949, 2022.
- [40] S. Liu, L. Mao, and J. Yu, “Path planning based on ant colony algorithm and distributed local navigation for multi-robot systems,” in *2006 International Conference on Mechatronics and Automation*, 2006, pp. 1733–1738.
- [41] P. Qin, Y. Fu, Y. Xie, K. Wu, X. Zhang, and X. Zhao, “Multi-agent learning-based optimal task offloading and UAV trajectory planning for AGIN-Power IoT,” *IEEE Transactions on Communications*, vol. 71, no. 7, pp. 4005–4017, 2023.
- [42] X. Wei, L. Cai, N. Wei, P. Zou, J. Zhang, and S. Subramaniam, “Joint UAV trajectory planning, DAG task scheduling, and service function deployment based on drl in UAV-empowered edge computing,” *IEEE Internet of Things Journal*, vol. 10, no. 14, pp. 12 826–12 838, 2023.
- [43] W. H. Yew, C. Fat Chau, A. W. Mahmood Zuhdi, W. Syakirah Wan Abdullah, W. K. Yew, and N. Amin, “Investigating the performance of deep reinforcement learning-based MPPT algorithm under partial shading condition,” in *2023 IEEE Regional Symposium on Micro and Nanoelectronics (RSM)*, 2023, pp. 9–12.
- [44] L. Mao, S. Liu, and J. Yu, “An improved ant colony algorithm for mobile robot path planning,” in *Journal of East China University of Science and Technology*, 2006, pp. 997–1001.
- [45] J. Liu, H. Weng, Y. Ge, S. Li, and X. Cui, “A self-healing routing strategy based on ant colony optimization for vehicular ad hoc networks,” *IEEE Internet of Things Journal*, vol. 9, no. 22, pp. 22 695–22 708, 2022.
- [46] I. Sakti, “Methodology of fuzzy logic with mamdani fuzzy models applied to the microcontroller,” in *2014 The 1st International Conference on Information Technology, Computer, and Electrical Engineering*, vol. 12, no. 17, 2014, pp. 93–98.
- [47] F. Marini and B. Walczak, “Particle swarm optimization (PSO). a tutorial,” *Chemometrics and Intelligent Laboratory Systems*, vol. 149, pp. 153–165, 2015.